THE JOURNAL OF PHYSICAL CHEMISTRY LETTERS
A JOURNAL OF THE AMERICAN CHEMICAL SOCIETY

pubs.acs.org/JPCL

Letter

Exceptionally Enhanced Thermal Conductivity of Aluminum Driven by Extreme Pressures: A First-Principles Study

Ashutosh Giri,* Pravin Karna, and Patrick E. Hopkins*

Cite This: *J. Phys. Chem. Lett.* 2022, 13, 10918−10923

Read Online

ACCESS | Metrics & More | Article Recommendations | Supporting Information

ABSTRACT: Extreme pressure conditions reveal fundamental insights into the physical properties of elemental metals that are otherwise not evident under ambient conditions. Herein, we use the density functional perturbation theory to demonstrate that the change in thermal conductivity as a result of large hydrostatic pressures at room temperature for aluminum is the largest of any known material. More specifically, in comparison to ambient conditions, we find that the change in thermal conductivity for aluminum is greater than the relative changes in thermal conductivities of diamond and cubic boron nitride combined, which are two of the most thermally conductive bulk materials known to date. We attribute this to the relatively larger increase in mean free paths and lifetimes of electrons in aluminum as a result of weaker electron−phonon coupling at higher pressures. Our work reveals direct insights into the exceptional electronic transport properties of pressurized aluminum and advances a broad paradigm for understanding thermal transport in metals under extreme pressure.

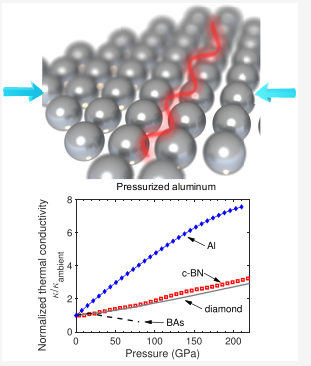

High-pressure studies provide insights into novel physical phenomena of the condensed state that are otherwise not discernible at ambient conditions. For example, high pressures have been utilized to effectively increase the superconducting transition temperature of elemental metals that are not superconducting at ambient pressure,[1−4] tune the thermal conductivity for different phases of materials over a wide range,[5−8] and increase thermal boundary conductance across two solids by increasing the interfacial bond stiffness.[9,10] In terms of the fundamental scattering mechanisms of the energy carriers, first-principles-based high-pressure studies on nonmetallic solids (far from pressure-induced phase transitions) have shown that phonon−phonon (p−p) scattering rates can either increase or decrease depending upon the available scattering phase space for the acoustic phonons.[8,11,12] Likewise, with the application of pressure on metallic solids, electron−phonon (e−p) interactions can either increase or decrease depending upon the type of electronic band structure.[2,13] These *ab initio*-based predictive studies lend critical insights into the unique phenomenon of condensed matter physics that are readily becoming accessible through high-pressure diamond anvil cell experiments with pressures reaching upward of 800 GPa.[14]

At ambient conditions, first-principles calculations based on the linear response theory have elucidated the spectral e−p coupling in several metals, demonstrating good agreement between tunneling experiments and theory.[15−18] Transport calculations based on the lowest order variational principle, which uses the spectral calculations as inputs to the simplifications of the Boltzmann transport equation (BTE) have also shown agreement with experimental results of electrical resistivities and thermal conductivities, thereby demonstrating the validity of the *ab initio* approaches.[13,16,19,20] Recently, the separate contributions from p−p and e−p scattering channels to the overall thermal conductivity of various types of metals have been calculated by solving the BTE in conjunction with density functional perturbation theory (DFPT) predictions carried out on dense meshes of phonon (q) and electron (k) wave vectors in the Brillouin zone.[21−23] Therefore, first-principles calculations offer the prospect of quantitatively analyzing the mode-level descriptions of microscopic mechanisms dictating energy transport and conversion between and within different energy carriers with high precision. This provides the opportunity for an in-depth and accurate understanding of the effect of the pressure on the various scattering mechanisms. However, to properly account for interactions between all electronic states and phonon modes in the entire Brillouin zone, fine meshes of phonon and electron wave vectors are necessary, especially at high pressures, to accurately predict the physical properties, such as electrical resistivities, heat capacities, and superconducting transition temperatures.[2,24,25] The recent developments in parameter-free first-principles-based calculations of p−p and e−p scattering mechanisms have enabled such types of calculations to be carried out in dense wave vector grids, thus offering a feasible route to the comprehensive under-

Received: October 10, 2022
Accepted: November 14, 2022
Published: November 17, 2022

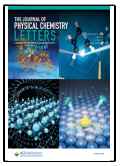

https://doi.org/10.1021/acs.jpclett.2c03090
J. Phys. Chem. Lett. 2022, 13, 10918−10923

standing of the microscopic mechanisms dictating energy transport in various types of materials.[26−28]

In this work, we calculate the thermal conductivity of Al under high pressures of up to ∼200 GPa by accounting for both e−p and p−p interactions from DFPT without any adjustable parameters. We find that the drastic decrease in e−p coupling with increasing pressure results in enhanced electronic thermal conductivities. The application of pressure is also shown to enhance phonon-driven thermal conductivity, which culminates to ∼20% of the total thermal conductivity at room temperature for pressures approaching 200 GPa, which is much higher in comparison to ∼5% contribution at ambient conditions. The contribution from lattice thermal conductivity is further enhanced to ∼50% of the total thermal conductivity at 100 K under hydrostatic pressures of 200 GPa and greater, suggesting that lattice vibrations can substantially contribute to heat conduction in metals for these conditions. At room temperature, our results reveal that the electron-driven changes in the thermal conductivity of Al are considerably larger in comparison to the changes observed for the lattice-driven thermal conductivities via pressure of some of the most thermally conductive and electrically insulative materials.

Our calculations of the e−p coupling are based on DFPT calculations as implemented in Quantum Espresso and the electron−phonon Wannier (EPW) packages.[25,29,30] The second- and third-order force constants for the calculations of p−p scattering are also determined by implementing Quantum Espresso and solving the iterative solution to the BTE. The strength of e−p coupling is generally represented by the e−p mass enhancement parameter, λ.[31] For accuracy, this parameter is calculated with dense electron and phonon wave vector grids utilizing the EPW package and is given as

$$\lambda = 2\int_0^\infty \frac{\alpha^2F(\omega)\mathrm{d}\omega}{\omega} \quad (1)$$

where ω is the phonon frequency and $\alpha^2F(\omega)$ is the Eliashberg function. Further details of the calculations are given in the Supporting Information. The calculations for λ as a function of the pressure (for pressures of up to 207 GPa) for Al are shown in Figure 1a. The application of ∼20 GPa hydrostatic pressure is shown to drastically reduce the coupling between the electronic and vibrational states, leading to ∼50% reduction in λ, whereas further application of the hydrostatic pressure causes modest reduction of λ, thereafter to ∼18% of the ambient value at pressures of up to 207 GPa.

In general, the application of pressure causes the spring constant between the atoms to stiffen and leads to the hardening of phonon modes, as shown in the phonon density of states for four different pressures in Figure 1b. The stiffening of the lattice is represented by the positive curvature of the relative volume change, and consequently, the maximum frequency increases monotonically with pressure (see Figure S2 of the Supporting Information). The maximum frequencies for both longitudinal and transverse polarizations monotonically increase (see Figure S4 of the Supporting Information) along with the reduction in the heights of the high-frequency peaks in the corresponding density of states (see Figure 1b). In contrast to the density of states, the peaks in the Eliashberg spectral function, $\alpha^2F(\omega)$, shift to higher frequencies, suggesting that electrons preferentially scatter with longitudinal phonons in Al for the entire pressure range, as shown in Figure 1c. Therefore, the reduction in the peak heights of the Eliashberg spectral function along with the stiffening of the phonon frequencies with pressure causes the e−p coupling (quantified by λ) to decrease, as shown in Figure 1a.

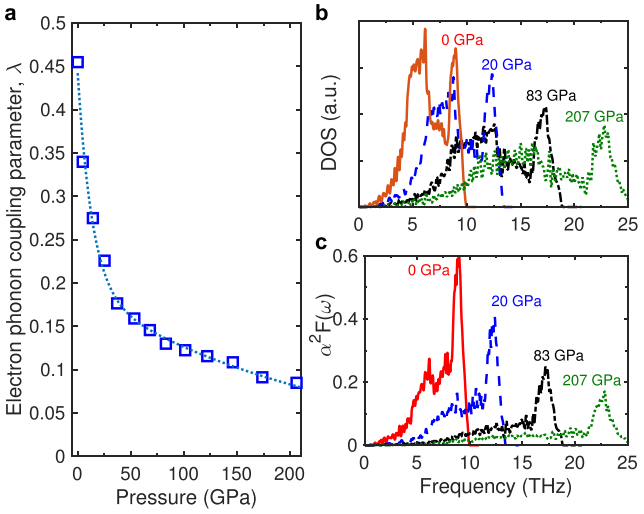

Figure 1. (a) Calculations of the electron−phonon coupling parameter (λ) versus applied hydrostatic pressure for Al from the density functional perturbation theory. The effect of the pressure is shown to drastically lower the electron−phonon scattering. (b) Phonon density of states for Al at four different pressures showing the monotonically increasing spectrum of frequencies as a result of application of hydrostatic pressure leading to lattice stiffening. (c) Calculated Eliashberg spectral functions [$\alpha^2F(\omega)$] at four different pressures. The effect of the hydrostatic pressure is shown to not only increase the maximum frequency but also shown to drastically lower the heights of the peaks in both the density of states and the spectral functions.

Before we consider the effect of the pressure on the overall thermal transport of Al as a result of e−p and p−p scattering mechanisms, we consider the changes in the heat capacities, Fermi velocities, phonon group velocities, and electron and phonon lifetimes with pressure. Figure 2a shows the calculated electron heat capacities and average Fermi velocities as a function of the pressure for Al. The application of pressure induces a slight increase in the heat capacities of the electrons and has a negligible influence on the Fermi velocity. Interestingly, the average Fermi velocity of $\sim 1.6 \times 10^6$ m s^{-1} at ambient obtained from our first-principles calculations deviates considerably from the predictions based on the free-electron theory ($\sim 2 \times 10^6$ m s^{-1}). This is surprising because Al possesses a free-electron-like electronic structure and the density of states follows the free electron gas model with a parabolic band dependence.[32] We note that our results are in-line with prior predictions from first-principles calculations of the mean free path of electrons in Al at ambient conditions.[33]

In comparison to the changes in Fermi velocities and electron heat capacities, the pressure-induced changes in the lifetimes and mean free paths of the electrons are much more pronounced for Al, as shown in Figure 2b, where we plot the average carrier lifetimes and mean free paths as a function of energy by accounting for e−p interactions at five different pressures. The average mean free path of electrons near the Fermi level is ∼16 nm with a lifetime of ∼10 fs at ambient conditions for Al, which are smaller than those for noble metals; for Ag and Au, the mean free paths of electrons near the Fermi level are ∼50 and ∼40 nm with lifetimes of ∼30 fs, respectively.[34] In comparison to the ambient pressure, the lifetimes and mean free paths of electronic energy states

https://doi.org/10.1021/acs.jpclett.2c03090
J. Phys. Chem. Lett. 2022, 13, 10918−10923

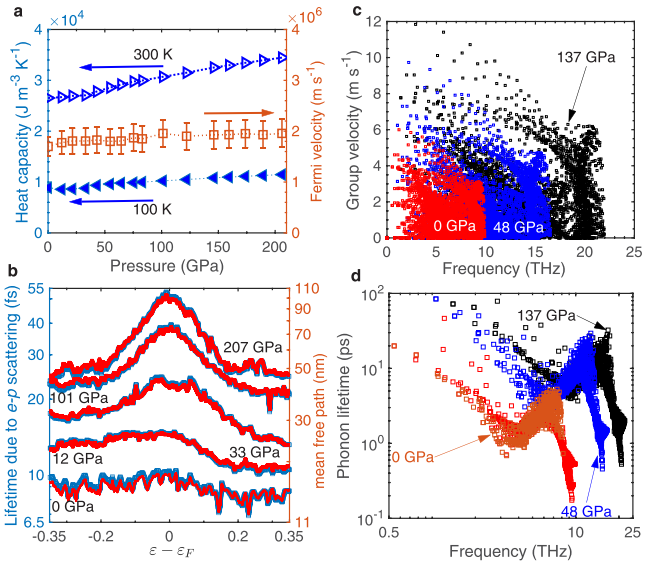

Figure 2. (a) Variation of the electronic heat capacity (at 100 and 300 K) and Fermi velocity with pressure for Al. The electronic heat capacity increases slightly with the pressure for the temperature range studied in this work, whereas the hydrostatic pressure has a negligible influence on the Fermi velocity. The Fermi velocity at ambient conditions (1.6×10^6 m s^{-1}) is ∼20% lower than the predictions of the free-electron theory (2×10^6 m s^{-1}). (b) Average electron lifetimes and mean free paths as a function of the electron energy for five different pressures. The left axis measures the lifetime (blue) and the right axis measures the mean free path (red) of electrons as a result of electron−phonon scattering. (c) Spectral phonon group velocity at three different pressures for Al. Along with broadening of the phonon spectrum, the group velocities of the phonon modes also increase with the pressure. (d) Spectral phonon lifetimes as a result of phonon−phonon scattering at three different pressures for Al.

around the Fermi level can increase by more than a factor of 5 with the application of ∼207 GPa hydrostatic pressure. Furthermore, the lifetimes are much longer for energy carriers near the Fermi level and are solely dictated by e−p interactions because, at the temperatures considered in this work, electron−electron interactions can safely be ignored.

In contrast to the electronic subsystem, the group velocities of the phonons increase for the entire vibrational spectrum with the application of hydrostatic pressure, as shown in Figure 2c. Therefore, unlike the electrons, the increase in the average group velocities of phonons has substantial contributions to the increase in the lattice thermal conductivity, as will be discussed in more detail below. Furthermore, the lifetimes of phonons are comparably longer and span a broader range compared to the lifetimes of electrons, as shown in Figure 2d. However, at ambient conditions, the phonon lifetimes are much shorter compared to that in a semiconductor, such as Si, which has an atomic mass similar to Al, but the strong covalent bonds and low anharmonicity give rise to longer phonon lifetimes and, therefore, higher phonon thermal conductivity in Si.[22] Surprisingly, the longest mean free paths of phonons in Al are similar to the mean free paths of electrons at ambient conditions (see Figure S5 of the Supporting Information). However, the mean free paths in the 1−10 nm range contribute ∼90% of the phonon thermal conductivity, whereas the range of mean free paths for electrons is much smaller, which validates the gray approximation to calculate electron-driven thermal conductivity, κ_e. As the pressure is increased, the lifetimes of phonons in Al increase and become comparable to that of the phonons in Si.[22]

Figure 3a shows the average lifetimes of electrons at the Fermi level as a function of the hydrostatic pressure for 100 and 300 K. The application of pressure monotonically increases the average lifetimes of electrons and leads to a qualitatively similar increase in the electron thermal conductivity, as shown in Figure 3b for the two temperatures. Although the lifetimes are higher at 100 K compared to 300 K, the electron thermal conductivity is higher at 300 K as a result of the larger electron heat capacity (see Figure 2a). This is in contrast to the $1/T$ dependence of lattice thermal conductivity, which is largely driven by anharmonic Umklapp scattering processes, as shown in Figure 3c at ambient pressure. For comparison, we also plot the separate contributions from κ_{ep} and κ_{pp} to the total thermal conductivity in Figure 3c. At room temperature, the contribution from κ_{pp} to the total thermal conductivity is ∼5% because the electrons are the dominant heat carriers at relatively higher temperatures. The contributions from κ_{pp} are greater at relatively lower temperatures. We also plot the experimentally measured temperature-dependent thermal conductivity of Al in Figure 3c. Our first-principles-based results match very well with the experimental results for temperatures of >150 K. However, at lower temperatures, our calculations underpredict the measured thermal conductivities considerably. This could be due to contributions from electron−electron scattering channels to the overall heat transport at lower temperatures, which have been ignored in our calculations and are beyond the scope of the current work but clearly deserve further investigations. At low temperatures, the lattice contribution increases with the application of pressure, as shown by the inset of Figure 3c for ∼82 GPa pressure and will be discussed in more detail below.

To quantitatively gauge the effect of the pressure on the relative contributions from κ_{pp} on the total thermal conductivity, we plot κ_{pp} and κ_{tot} as a function of the prescribed hydrostatic pressure for 100 and 300 K in Figure 3d. Although κ_{pp} at 100 K is higher than at 300 K, the total thermal conductivities from e−p and p−p scattering mechanisms are similar at the two temperatures. Furthermore, the contributions from κ_{pp} to the overall thermal conductivity increase from 5% at ambient to ∼18% at 300 K, as shown in Figure 3e. The phonon contributions to κ_{tot} are increased at 100 K for all pressures with an increase from ∼20 to 50% from ambient pressure to 207 GPa hydrostatic pressure. This suggests that the lattice contributions to thermal conductivity in Al cannot be ignored at high pressures.

In Figure 4a, we compare the pressure-dependent total thermal conductivity of Al with three semiconductors (i.e., diamond, cubic boron nitride, and boron arsenide) with some of the highest known thermal conductivities at room temperature determined via first-principles-based calculations.[8,11,12] Not surprisingly, the thermal conductivity of the isotopically pure diamond as calculated by Broido et al.[11] represents the highest attainable thermal conductivity throughout the pressure range for any known material. The first-principles-predicted thermal conductivity of cubic boron nitride (c-BN) follows the qualitative monotonic increase in thermal conductivity of a diamond with slightly lower values.[12] The monotonic enhancement is attributed to stiffening of the phonons with acoustic velocities and reduced p−p scattering rates. Moreover, the increase in optic mode frequencies with pressure in these insulators is shown to weaken the coupling

https://doi.org/10.1021/acs.jpclett.2c03090
J. Phys. Chem. Lett. 2022, 13, 10918−10923

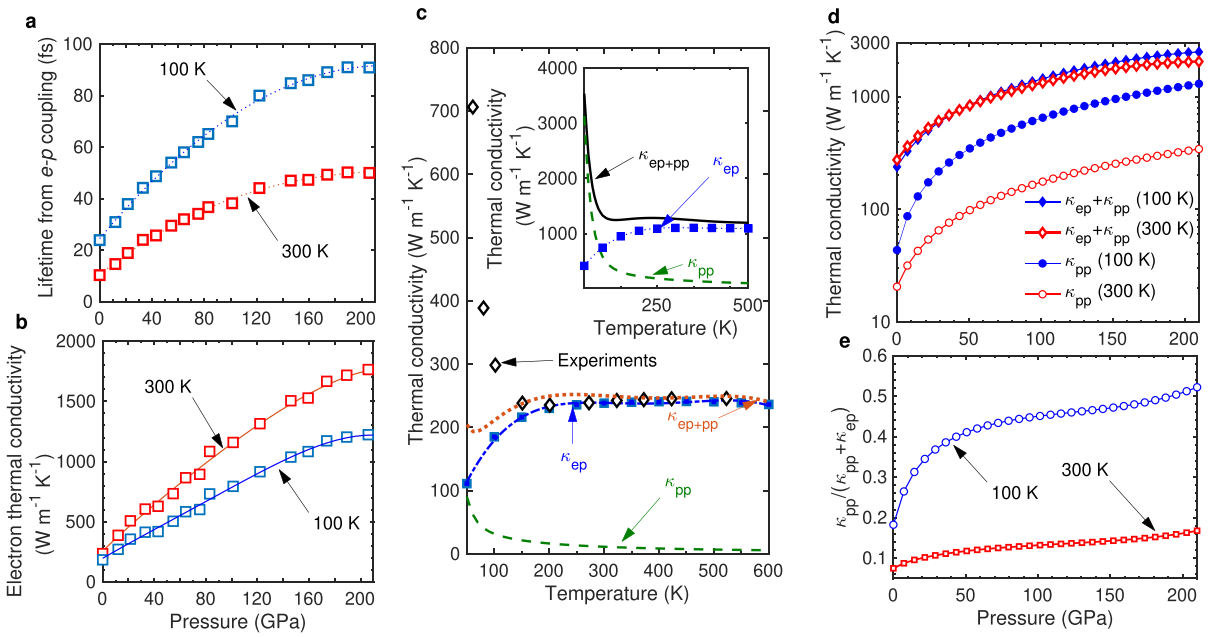

Figure 3. (a) Average lifetime for electrons as a result of electron−phonon scattering at the Fermi level as a function of the applied hydrostatic pressure for 100 and 300 K. The lifetimes increase monotonically for pressures up to ∼100 GPa and start to plateau at higher pressures. (b) Calculated electron thermal conductivity for 100 and 300 K versus hydrostatic pressure. The electron thermal conductivity shows trends similar to the electron lifetimes at the two different temperatures. Even though the lifetimes are higher at lower temperatures, the electron thermal conductivities are higher at 300 K compared 100 K as a result of the larger electronic heat capacities at higher temperatures. (c) Temperature-dependent thermal conductivity as a result of electron−phonon (blue squares) and phonon−phonon (green dashed line) scattering mechanisms at ambient pressure. The total thermal conductivity as a result of the two mechanisms is also shown (red dotted line). For comparison, we also plot the experimental thermal conductivity of Al taken from ref 35, which shows remarkable agreement with our first-principles-based calculations for relatively higher temperatures (>200 K). (Inset) Temperature-dependent thermal conductivity as a result of electron−phonon (blue squares), phonon−phonon (green dashed line), and total thermal conductivity (black line) for Al at 82 GPa. (d) Thermal conductivity as a result of electron−phonon and phonon−phonon scattering as a function of the pressure for two different temperatures. (e) Phonon-driven thermal conductivity normalized by the total thermal conductivity as a function of the pressure for 100 and 300 K. The lattice contribution to the total thermal conductivity is higher at 100 K compared to room temperature and can reach ∼50% at extreme pressure conditions.

with the heat carrying acoustic modes, thus leading to the increase in the lattice thermal conductivity.[11] In contrast, a nonmonotonic decrease at high pressures is predicted for BAs, which has been attributed to the large mass difference between the constituent atoms in the unit cell of BAs, leading to significant frequency gaps between acoustic and optic phonons.[8] More specifically, Lindsay et al.[8] have shown that as a result of the significant gap between the acoustic and optic phonon modes, the three phonon scattering processes are exclusively dominated by acoustic modes for which the scattering phase space increases as a result of hardening of acoustic modes with pressure. This leads to the reduction of thermal conductivity with pressure in BAs. In comparison to these electrical insulators, the electron-dominated thermal conductivity of Al surpasses that of BAs at higher pressures and shows a monotonic increase similar to a diamond and c-BN, even though the quantitative values are lower than these insulators for the entire pressure range. However, the unique pressure dependence of thermal conductivity in Al is observed when we compare its relative increase from ambient conditions. In Figure 4b, we plot the normalized thermal conductivity with respect to the thermal conductivity at ambient pressure as a function of the hydrostatic pressure for Al, diamond, c-BN, and BAs. The thermal conductivity of Al at 207 GPa is ∼8× higher than that at ambient pressure, whereas the increase for a diamond and c-BN is only ∼3×. The higher rate of increase in the thermal conductivity for Al with pressure is a direct consequence of the large increase in electron lifetimes, as discussed above, demonstrating the larger tunability of electron-driven thermal properties with external stimuli compared to the phonon-driven processes in semiconductors. We note that, while metals, such as Al, Ag, and Au, demonstrate a decreasing e−p coupling strength with pressure,[13] some metals, such as K and Li, show an increasing trend in e−p coupling strength for a range of pressure conditions.[2] This suggests that the electron-driven thermal conductivity increases with pressure as a result of reduced e−p coupling that we observe for Al in this work might not be generalized to all metals. Moreover, for some transition metals, such as Ni and W, the purely phonon-driven thermal conductivity has a more significant contribution to the total thermal conductivity in comparison to Al.[21,36] As such, the drastically increased electron thermal conductivity that we observe for aluminum might not be transferable to those metals. Therefore, a detailed investigation of both phonon and electron thermal conductivities utilizing dense electron and phonon wave vector grids for accurate predictions of the e−p scattering matrix should be carried out for all metals to fully understand their pressure-dependent thermal conductivities.

In summary, we have demonstrated the unique pressure dependence of aluminum; i.e., the relative change in the thermal conductivity as a result of large hydrostatic pressures at room temperature for aluminum is the largest of any known material. More specifically, in comparison to ambient conditions, we find that the change in thermal conductivity for aluminum is greater than the relative changes in the

https://doi.org/10.1021/acs.jpclett.2c03090
J. Phys. Chem. Lett. 2022, 13, 10918−10923

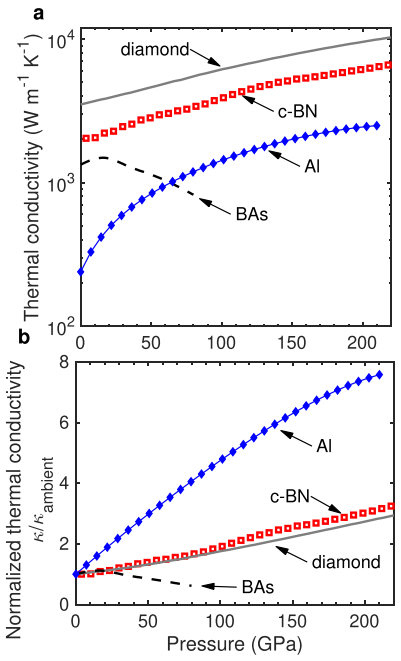

Figure 4. First-principles-based calculations of thermal conductivity versus pressure for diamond (ref 11), cubic BN (ref 12), cubic BAs (ref 8), and Al (this work). (b) Normalized thermal conductivity with respect to the ambient thermal conductivity for the different materials as a function of the pressure. The relative increase in thermal conductivity of Al is much larger compared to the phonon-driven increase in thermal conductivity of a diamond and cubic BN, which are the two most thermally conductive materials to date.

thermal conductivities of a diamond and cubic boron nitride combined, which are two of the most thermally conductive bulk materials known to date. Our results reveal the enhanced potential of tuning the electron-driven thermal conductivity of metals via pressure compared to pressure-dependent changes in the lattice thermal conductivity of electrical insulators at moderate temperatures (from ∼100 to 600 K) studied in this work. We attribute this to the relatively larger increase in the mean free paths and lifetimes of electrons in aluminum as a result of weaker electron−phonon coupling at higher pressures. Furthermore, at hydrostatic pressures of ∼200 GPa, the contributions from the lattice thermal conductivity in aluminum increases from ∼20 to ∼50% as the temperature decreases from 300 to 100 K, suggesting that the lattice contributions cannot be ignored in aluminum with the application of large hydrostatic pressures.

■ ASSOCIATED CONTENT

Supporting Information

The Supporting Information is available free of charge at https://pubs.acs.org/doi/10.1021/acs.jpclett.2c03090.

Details of density functional perturbation theory calculations, electron−phonon coupling, and electron- and phonon-driven thermal conductivities (PDF)

■ AUTHOR INFORMATION

Corresponding Authors

Ashutosh Giri − *Department of Mechanical and Aerospace Engineering, University of Virginia, Charlottesville, Virginia 22904, United States;* orcid.org/0000-0002-8899-4964; Email: ashgiri@uri.edu

Patrick E. Hopkins − *Department of Mechanical and Aerospace Engineering, University of Virginia, Charlottesville, Virginia 22904, United States; Department of Materials Science and Engineering and Department of Physics, University of Virginia, Charlottesville, Virginia 22904, United States;* orcid.org/0000-0002-3403-743X; Email: phopkins@virginia.edu

Author

Pravin Karna − *Department of Mechanical, Industrial and Systems Engineering, University of Rhode Island, Kingston, Rhode Island 02881, United States*

Complete contact information is available at: https://pubs.acs.org/10.1021/acs.jpclett.2c03090

Notes

The authors declare no competing financial interest.

■ ACKNOWLEDGMENTS

This work is supported by the Office of Naval Research (Grants N00014-21-1-2622 and N00014-22-1-2139).

■ REFERENCES

(1) Hamlin, J. Superconductivity in the Metallic Elements at High Pressures. *Phys. C: Supercond. and its Appl.* **2015**, *514*, 59−76.

(2) Profeta, G.; Franchini, C.; Lathiotakis, N. N.; Floris, A.; Sanna, A.; Marques, M. A. L.; Lüders, M.; Massidda, S.; Gross, E. K. U.; Continenza, A. Superconductivity in Lithium, Potassium, and Aluminum Under Extreme Pressure: A First-Principles Study. *Phys. Rev. Lett.* **2006**, *96* (4), 047003.

(3) Ashcroft, N. W. Putting the Squeeze on Lithium. *Nature* **2002**, *419* (6907), 569−571.

(4) Sakata, M.; Nakamoto, Y.; Shimizu, K.; Matsuoka, T.; Ohishi, Y. Superconducting State of Ca-VII below a Critical Temperature of 29 K at a Pressure of 216 GPa. *Phys. Rev. B* **2011**, *83* (22), 220512.

(5) Dalton, D. A.; Hsieh, W.-P.; Hohensee, G. T.; Cahill, D. G.; Goncharov, A. F. Effect of Mass Disorder on the Lattice Thermal Conductivity of MgO Periclase Under Pressure. *Sci. Rep.* **2013**, *3* (1), 2400.

(6) Hsieh, W.-P.; Chen, B.; Li, J.; Keblinski, P.; Cahill, D. G. Pressure Tuning of the Thermal Conductivity of the Layered Muscovite Crystal. *Phys. Rev. B* **2009**, *80* (18), 180302.

(7) Giri, A.; Hopkins, P. E. Pronounced Low-frequency Vibrational Thermal Transport in C_{60} Fullerite Realized through Pressure-dependent Molecular Dynamics Simulations. *Phys. Rev. B* **2017**, *96* (22), 220303.

(8) Lindsay, L.; Broido, D. A.; Carrete, J.; Mingo, N.; Reinecke, T. L. Anomalous Pressure Dependence of Thermal Conductivities of Large Mass Ratio Compounds. *Phys. Rev. B* **2015**, *91* (12), 121202.

(9) Hohensee, G. T.; Wilson, R. B.; Cahill, D. G. Thermal Conductance of Metal−Diamond Interfaces at High Pressure. *Nat. Commun.* **2015**, *6* (1), 6578.

(10) Hsieh, W.-P.; Lyons, A. S.; Pop, E.; Keblinski, P.; Cahill, D. G. Pressure Tuning of the Thermal Conductance of Weak Interfaces. *Phys. Rev. B* **2011**, *84* (18), 184107.

(11) Broido, D. A.; Lindsay, L.; Ward, A. Thermal Conductivity of Diamond Under Extreme Pressure: A First-principles Study. *Phys. Rev. B* **2012**, *86* (1), 115203.

(12) Ravichandran, N. K.; Broido, D. Non-Monotonic Pressure Dependence of the Thermal Conductivity of Boron Arsenide. *Nat. Commun.* **2019**, *10* (1), 827.

(13) Giri, A.; Gaskins, J. T.; Li, L.; Wang, Y.-S.; Prezhdo, O. V.; Hopkins, P. E. First-principles Determination of the Ultrahigh Electrical and Thermal Conductivity in Free-electron Metals via Pressure Tuning the Electron-Phonon Coupling Factor. *Phys. Rev. B* **2019**, *99* (16), 165139.

(14) Bradley, D. K.; Eggert, J. H.; Smith, R. F.; Prisbrey, S. T.; Hicks, D. G.; Braun, D. G.; Biener, J.; Hamza, A. V.; Rudd, R. E.; Collins, G. W. Diamond at 800 GPa. *Phys. Rev. Lett.* **2009**, *102* (7), 075503.
(15) Savrasov, S. Y.; Savrasov, D. Y.; Andersen, O. K. Linear-Response Calculations of Electron-Phonon Interactions. *Phys. Rev. Lett.* **1994**, *72* (3), 372−375.
(16) Savrasov, S. Y.; Savrasov, D. Y. Electron-Phonon Interactions and Related Physical Properties of Metals from Linear-Response Theory. *Phys. Rev. B* **1996**, *54* (23), 16487−16501.
(17) Savrasov, S. Y. Linear-Response Theory and Lattice Dynamics: A Muffin-Tin-Orbital Approach. *Phys. Rev. B* **1996**, *54* (23), 16470−16486.
(18) Bauer, R.; Schmid, A.; Pavone, P.; Strauch, D. Electron-Phonon Coupling in the Metallic Elements Al, Au, Na, and Nb: A First-Principles Study. *Phys. Rev. B* **1998**, *57* (18), 11276−11282.
(19) Bauer, M.; Pawlik, S.; Aeschlimann, M. Electron Dynamics of Aluminum Investigated by Means of Time-Resolved Photoemission. Laser Techniques for Surface Science III. *Proc. SPIE* **1998**, *3272*, 201−210.
(20) Giri, A.; Tokina, M.; Prezhdo, O.; Hopkins, P. Electron−Phonon Coupling and Related Transport Properties of Metals and Intermetallic Alloys from First Principles. *Mater. Today Phys.* **2020**, *12*, 100175.
(21) Tong, Z.; Li, S.; Ruan, X.; Bao, H. Comprehensive First-Principles Analysis of Phonon Thermal Conductivity and Electron-Phonon Coupling in Different Metals. *Phys. Rev. B* **2019**, *100* (14), 144306.
(22) Jain, A.; McGaughey, A. J. H. Thermal transport by Phonons and Electrons in Aluminum, Silver, and Gold from First Principles. *Phys. Rev. B* **2016**, *93* (8), 081206.
(23) Wang, Y.; Lu, Z.; Ruan, X. First Principles Calculation of Lattice Thermal Conductivity of Metals Considering Phonon-Phonon and Phonon-Electron Scattering. *J. Appl. Phys.* **2016**, *119* (22), 225109.
(24) Bazhirov, T.; Noffsinger, J.; Cohen, M. L. Superconductivity and Electron-Phonon Coupling in Lithium at High Pressures. *Phys. Rev. B* **2010**, *82* (18), 184509.
(25) Poncé, S.; Margine, E.; Verdi, C.; Giustino, F. EPW: Electron-Phonon Coupling, Transport and Superconducting Properties using Maximally Localized Wannier Functions. *Comput. Phys. Commun.* **2016**, *209*, 116−133.
(26) McGaughey, A. J. H.; Jain, A.; Kim, H.-Y.; Fu, B. Phonon Properties and Thermal Conductivity from First Principles, Lattice Dynamics, and the Boltzmann Transport Equation. *J. Appl. Phys.* **2019**, *125* (1), 011101.
(27) Lindsay, L.; Katre, A.; Cepellotti, A.; Mingo, N. Perspective on Ab Initio Phonon Thermal Transport. *J. Appl. Phys.* **2019**, *126* (5), 050902.
(28) Giustino, F. Electron-Phonon Interactions from First Principles. *Rev. Mod. Phys.* **2017**, *89* (1), 015003.
(29) Giannozzi, P.; Baroni, S.; Bonini, N.; Calandra, M.; Car, R.; Cavazzoni, C.; Ceresoli, D.; Chiarotti, G. L; Cococcioni, M.; Dabo, I.; Dal Corso, A.; de Gironcoli, S.; Fabris, S.; Fratesi, G.; Gebauer, R.; Gerstmann, U.; Gougoussis, C.; Kokalj, A.; Lazzeri, M.; Martin-Samos, L.; Marzari, N.; Mauri, F.; Mazzarello, R.; Paolini, S.; Pasquarello, A.; Paulatto, L.; Sbraccia, C.; Scandolo, S.; Sclauzero, G.; Seitsonen, A. P; Smogunov, A.; Umari, P.; Wentzcovitch, R. M QUANTUM ESPRESSO: A Modular and Open-Source Software Project for Quantum Simulations of Materials. *J. Phys.: Condens. Matter* **2009**, *21*, 395502.
(30) Noffsinger, J.; Giustino, F.; Malone, B. D.; Park, C.-H.; Louie, S. G.; Cohen, M. L. EPW: A Program for Calculating the Electron-Phonon Coupling Using Maximally Localized Wannier Functions. *Comput. Phys. Commun.* **2010**, *181* (12), 2140−2148.
(31) Allen, P. B. Theory of Thermal Relaxation of Electrons in Metals. *Phys. Rev. Lett.* **1987**, *59* (13), 1460−1463.
(32) Kittel, C. *Introduction to Solid State Physics*, 6th ed.; John Wiley & Sons, Inc.: New York, 1986.
(33) Gall, D. Electron Mean Free Path in Elemental Metals. *J. Appl. Phys.* **2016**, *119* (8), 085101.
(34) Brown, A. M.; Sundararaman, R.; Narang, P.; Goddard, W. A.; Atwater, H. A. Nonradiative Plasmon Decay and Hot Carrier Dynamics: Effects of Phonons, Surfaces, and Geometry. *ACS Nano* **2016**, *10* (1), 957−966.
(35) Klemens, P. In *Metals: Electronic Transport Phenomena*; Hellwege, K.-H., Olsen, J. L., Eds.; Springer-Verlag: Berlin, Germany, 1982; Vol. *15*.
(36) Chen, Y.; Ma, J.; Li, W. Understanding the Thermal Conductivity and Lorenz Number in Tungsten from First Principles. *Phys. Rev. B* **2019**, *99* (2), 020305.

https://doi.org/10.1021/acs.jpclett.2c03090
J. Phys. Chem. Lett. 2022, 13, 10918−10923